International Journal of Thin Films Science and Technology

http://dx.doi.org/10.18576/ijtfst/150107

Exploring the Interplay Between Composition and Milling Duration on the Microstructure and Mechanical Properties of XNiCrAlY + Y(NiCr-CrC) Composite Coatings

Andrieanto Nurrochman[1,], Endro Junianto[2], Akhmad A. Korda[1], Djoko H. Prajitno[3], Budi Prawara[2], and Eddy A. Basuki[1]*

[1] Metallurgical Engineering Research Group, Faculty of Mining and Petroleum Engineering, Institut Teknologi Bandung, Bandung, 40132, Indonesia
[2] Research Center for Advanced Materials, National Research and Innovation Agency (BRIN), Serpong, 15314, Indonesia
[3] Metallurgical Engineering, Faculty of Manufacturing Technology. Universitas Jendral Achmad Yani, Bandung, 40285, Indonesia

Received: 12 Oct. 2025, Revised: 22 Nov. 2025, Accepted: 12 Dec. 2025
Published online: 1 Jan. 2026

Abstract: This study explores the development of XNiCrAlY + Y(NiCr-CrC) HVOF-deposited composite coatings. The feedstock powders were formulated with varying weight ratios of NiCrAlY and Ni-CrC and subjected to mechanical milling between 2 and 36 hours to refine the particle size. Findings demonstrated that moderate milling times enhanced the hardness and wear resistance of the coatings. However, extended milling beyond 12 hours led to in-flight oxidation, which can impair the effectiveness of the milled powder's deposition. This oxidation also compromises the inter-splat bonding, resulting in a more porous and less cohesive coating structure. Furthermore, the interplay between the NiCrAlY/NiCr-CrC composition ratios and milling duration significantly influences coating characteristics, emphasizing the necessity of precisely tailoring these parameters for optimum performance. It points to the potential of NiCrAlY + (NiCr-CrC) coatings to enhance the durability and sustainability of materials.

Keywords: Thermal spray coating, HVOF, NiCr-CrC coatings, Mechanical milling, Mechanical properties.

1 Introduction

Reducing CO_2 emissions from fossil-based power plants is a critical aspect of the global effort to combat climate change. Power plants are one of the most significant sources of CO_2 emissions, and enhancing their efficiency is essential to mitigate their environmental impact. A principal strategy for achieving a more environmentally friendly power plant is to improve thermodynamic efficiency, which involves increasing the operating temperature and pressure, such as in ultra-supercritical (USC) boilers [1,2]. However, these extreme conditions introduce significant challenges, particularly concerning the integrity of boiler materials in USC power plants. Boiler tubes erode as hot flue gases pass through them, carrying abrasive particles. It mainly attacks the tube side walls, reducing their thickness and eventually causing the components to fail [3-7]. Consequently, protective measures must be urgently implemented to ensure the longevity, reliability, and safety of these components.

Over the past decades, coatings have gained popularity as a reliable strategy for increasing the service life in erosive high-temperature environments [8-10]. Thermal spray coating technology, in particular, can significantly improve abrasion and erosion resistance. For instance, high-velocity oxygen-fuel (HVOF) sprayed tungsten carbide (WC) based coatings are renowned for their exceptional hardness and resistance against wear caused by abrasion and erosion [11,12]. Typically, WC-based coatings formed a composite with Co as a binder matrix [13]. The WC particles have a high hardness and brittleness, whereas the metallic matrix combines strength and ductility. This combination yields a material with distinct properties, including high hardness and good fracture toughness [14]. However, their application in high temperature environments, such as those found in USC boilers, is limited by fundamental drawbacks [15]. First is that WC-Co has a coefficient of thermal expansion (CTE) significantly smaller than that of the steel substrate (WC(CTE) = $6.9 \times 10^{-6}\ K^{-1}$ [16] and steel (CTE) = $11 - 12 \times 10^{-6}\ K^{-1}$ [17]). This mismatch induces substantial thermal stresses, often leading to the formation of cracks in the coating when exposed to high temperatures. The other is WC–Co exhibited a significant strength loss after oxidation due to a smaller load-bearing section and several intrinsic effects, such as larger flaws, oxide wedging, and residual stress.

Nickel chrome-chromium carbide (NiCr-CrC) based coatings were developed to address the aforementioned issues [17]. These coatings offer a much closer match in CTE with the steel substrate and exhibit better thermal

*Corresponding author E-mail: andrieanto@unisba.ac.id

stability than the WC-based coating [18,19]. Moreover, thermal spray coatings of NiCr-CrC are quite attractive because of their ability to increase wear and corrosion resistance at high temperatures [20-22]. The hardness of the carbide particles enhances wear resistance, while the NiCr matrix provides corrosion resistance. These coatings have found widespread use in protecting boiler tubes. Nevertheless, in aggressive corrosive environments, especially those involving salt deposits at high temperatures, the hot corrosion resistance of NiCr-CrC coatings remains inferior to that of alumina-forming alloy coatings. Research has shown that a protective Al_2O_3 layer on the coating [23] offers superior protection under high-temperature conditions.

One of the alumina-forming alloys is the family of MCrAlY (M=Ni, Co, or NiCo) coatings. During the high temperature exposure, the selective oxidation of aluminum in the alloy forms a dense, stable Al_2O_3 on the surface. This oxide acts as an effective diffusion barrier, protecting against corrosive salt species [24]. However, MCrAlY coatings possess relatively low hardness and poor intrinsic resistance to mechanical wear, such as solid particle erosion [25]. A significant fraction of reinforcing is required to increase the wear performance of MCrAlY coatings.

The inherent limitations of these coatings suggest a composite approach that combines the distinct advantages of coatings from different materials. A composite coating of MCrAlY + (NiCr-CrC) has been developed. This composite coating offers a balance of high hot corrosion resistance of an alumina-former, and sufficient mechanical properties of a cermet [26,27]. Studies have shown that applying this composite coating enhances corrosion resistance [26]. However, the performance of such a composite is highly dependent on its microstructure [28]. The final coating performance is critically dependent on the microstructural architecture, such as the size, distribution, and morphology of the constituent phases, as well as the nature of the interfaces between them. These microstructural features are, in turn, dictated by the characteristics of the feedstock powder and the deposition process parameters.

In recent years, nanostructured coatings have attracted significant research due to their promising benefits, resulting in better mechanical properties than conventional ones [29-31]. Mechanical milling is recognized as a robust top-down process to generate a refined structure down to the nanoscale [32]. Mechanically milled HVOF NiCr-CrC powder has significantly improved the performance of its coatings [33-36]. Nanostructured NiCr-CrC coatings exhibit a more uniform microstructure with fine carbide particles well dispersed throughout the metallic matrix [31]. This coating structure is expected to improve its mechanical properties and corrosion resistance compared to conventional coatings [29,30]. Furthermore, the nanostructured NiCr-CrC coating possessed a denser structure than the conventional one. Similarly, a refined nanostructure of NiCrAlY can promote the formation of a dense and uniform oxide layer, thereby improving its corrosion resistance [37]. Nonetheless, Kevin J Stein et al. [38] proposed that a significant amount of carbide-based particles as a strengthener is still required to boost the wear resistance of the M(Ni, Co)CrAlY coating.

While extensive research has been done on the nanostructured NiCr-CrC and MCrAlY individually [39,40], understanding how the properties of a mixed NiCrAlY + NiCr-CrC are affected by both the composite ratio and the mechanical milling duration has not been reported. Here, we pioneer an approach to co-optimizing both powder composition ratio and milling process to explore the complex relationship between grain refinement advantages and the effect of powder refinement processing. This study aims to elucidate the microstructural evolution of the composite coatings under varying their compositions and milling duration. The interplay between the coating's mechanical properties and its composition, as well as the processing parameters, will be investigated thoroughly.

2 Experimental Details

2.1 Powder Preparation

Two types of starting materials were employed. The First was a commercially available amdry 962 NiCrAlY powder by Oerlikon Metco, manufactured through gas atomization, resulting in a spheroidal shape with particle size distribution of -106 +53 µm. The second was a commercial MEC-GP-25-588 NiCr-Cr3C2 blend powder provided by Metallizing Equipment Co. Pvt. Ltd., which had a more equiaxed shape and a particle size distribution of -45 + 10 µm.

The detailed synthesized composite composition of the feedstock powders and the composition of the starting materials are shown in Table 1. The notation used in this study of XNiCrAlY + Y(NiCr-CrC) corresponds to the powder weight percentages, with X referring to the NiCrAlY powder weight percentage and Y referring to the NiCr-CrC powder weight percentage. Therefore, Sample A(n) denotes the composition of 50 wt.% (NiCr-CrC) + 50 wt.% NiCrAlY with X=50 and Y=50. Similarly, Sample B(n) denotes the composition of 75 wt.% (NiCr-CrC) + 25 wt.% NiCrAlY with X=25 and Y=75. The n in the parentheses denotes the milling duration in hours.

Table 1: Feedstock powder composition

Sample code	Composite powder composition	Starting materials chemical composition
A(n*)	50 wt.% (NiCr-CrC) + 50 wt.% NiCrAlY	NiCrAlY (Ni (Bal); Cr (21.0 – 23.0 wt.%); Al (9.0 – 11.0 wt.%); Y (0.8 – 1.2 wt.%)
B(n*)	75 wt.% (NiCr-CrC) + 25 wt.% NiCrAlY	NiCr-CrC (25 wt% NiCr with Ni (20 wt%); Cr (Bal.) + 75 wt% Cr_3C_2)

*n is the milling time denoted with 2, 12, 22, and 36

Composite feedstock powders were mechanically milled with the high speed planetary ball mill to reduce the particle size (Model-PQ-N2 Gear Drive 4-station, Across International, United States of America). The vial and ball used for milling were made of alumina. The vial has a 500 ml volume, and the ball is 3 mm in diameter. The milling process was conducted at room temperature, with the milling vial filled with high-purity argon gas to minimize oxidation of the powder mixture. To prevent excessive vial overheating, the milling process was conducted by alternating 60 minutes of milling followed by 10 minutes of relaxation. The key milling parameters are mentioned in Table 2, and the total weight of powder composition obtained was 200 g. Prior to coating, the substrate's surface was prepared by grinding it up to 1500 grit using SiC-based abrasive paper. Then, the substrates were blasted with 24 mesh alumina grit to enhance adhesion and remove surface contaminants. Each step of substrate surface preparation was followed by acetone cleaning. Preheating was performed on the substrate using the HVOF gun, up to approximately 100 °C, just before the deposition process. The thermal spraying was conducted using a Tecknotherm HVOF 2007 thermal spray machine and Hipojet-2700 spray gun. The spraying distance was maintained at 200 mm with a 90 ° angle between the gun and the substrates. The details of the HVOF parameter can be seen in Table 3.

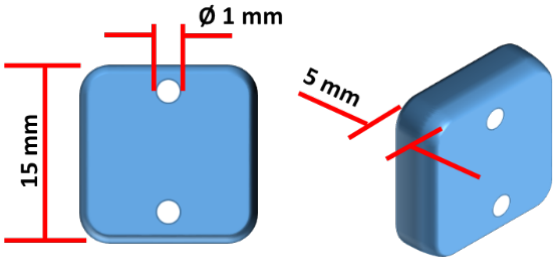

Fig. 1: Substrate dimension illustration

Table 2: Milling parameters each milled composite

Parameter	Value
Ball-to-powder mass ratio	20:1
Process control agent	Stearic acid (1 wt%)
Rotational speed (rpm)	250
Milling time (h)	2, 12, 22, 36

2.2 Coating Deposition

The substrate material used for coating deposition was 304 stainless steels with dimensions as illustrated in Figure 1.

Table 3: HVOF deposition parameter

Parameter	Value
Oxygen pressure (bar)	8
Oxygen flow rate (L/min)	270
Propane pressure (bar)	5.5
Propane flow rate (L/min)	62.4
Nitrogen pressure (bar)	5
Nitrogen flow rate (L/min)	8
Air pressure (bar)	6.2

2.3 Characterization

The morphology of the powders and the coating microstructure were observed using scanning electron microscopy (SEM, JEOL JSM-IT300LA) equipped with energy dispersive spectroscopy (EDS, X-MaxN, Oxford). Powder phase identification was conducted by X-ray diffraction (XRD, Rigaku Smartlab) with Cu Kα radiation.

2.4 Abrasive wear and microhardness test

The wear tests were performed using a Pin-on-Disc instrument in accordance with the American Society for Testing and Materials (ASTM) G99-06 standard. The tests were conducted at room temperature with a contact pressure of 1 MPa and a sliding velocity of 1.57 m/s for 30 min. A spherical ball of WC pin with a diameter of 3 mm was used. The wear behavior was evaluated by the weight loss measurement using an analytical balance with a precision of 10−4 g.

The microhardness of the HVOF coating was measured using a Metkon Duroline M microhardness tester with a load of 200 gf and a dwell duration of 10 seconds on a polished cross-section surface. Six data points were collected across the substrate to the coating, with three times indentation. Each data point was collected and averaged for each hardness number.

3 Results and discussion

3.1 Morphological Characteristics of the Milled Composite Feedstock Powder

The milled composite powders were collected at each milling time to observe their morphological characteristics. Figure 2 shows the SEM morphological observations of the milled composite powder as a function of milling time and composition.

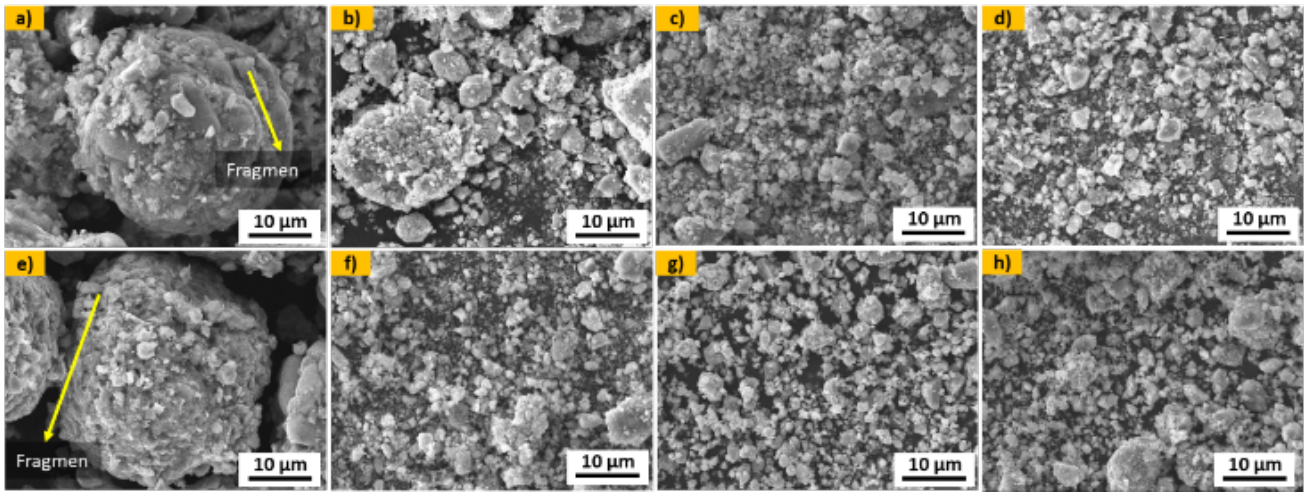

Fig. 2: Morphological evolution of the composite feedstock powder for (a) A(2), (b) A(12), (c) A(22), (d) A(36), (e) B(2), (f) B(12), (g) B(22), and (h) B(36).

Mechanical milling induced significant changes in the morphology of the powders, as shown in the SEM observations. The evolution of the powders is governed by milling mechanisms that involve a continuous and competing process of cold welding and fracture, particularly in systems containing both ductile and brittle components.

At the initial 2 hours of milling, smaller, fragmented brittle NiCr-CrC are observed adhering to the surfaces of the larger, more ductile NiCrAlY particles (Figure 2a, 2e). During the intense collisions in the milling process, the ductile NiCrAlY particles undergo significant plastic deformation, while the brittle NiCr-Cr-C particles fracture and are fragmented. The deformed surfaces of NiCrAlY particles are highly reactive, facilitating the cold welding of these brittle fragments onto their surfaces [41]. Therefore, the particle size distribution will be significantly affected.

The size distribution of the milled composite powders, as depicted in a Gaussian fit, can be seen in Figure 3a. Generally, the composite powders have a smaller particle size distribution than the initial size after milling for 2 to 36 hours. Figure 3b presents the evolution of median particle size (D50) with respect to milling duration. The trends of the size reduction for the two powder compositions are quite similar, with both experiencing an increase in D50 from 2 to 12 hours of milling. The D50 value then decreases as milling time increases, reaching near steady state condition after 22 hours.

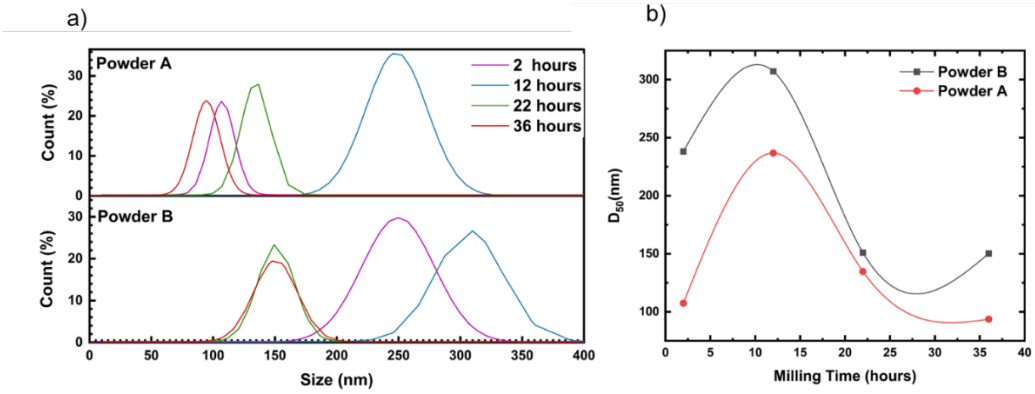

Fig. 3: (a) Particle size distribution of the milled composite powder; (b) D50(nm) size of the milled composite powder

This trend, which is quite typical for ductile-brittle powder systems [41], can be attributed to the dominance of cold welding over particle fracture during the initial milling stages as observed in the SEM. In this context, the ductile NiCrAlY phase essentially serves as a binder, incorporating the fractured NiCr–CrC particles into progressively larger composite agglomerates. As the milling time continues, the ductile NiCrAlY particles undergo notable work hardening when subjected to sustained, intense plastic deformation, resulting in increased hardness but a loss in ductility.[42,43] The particles reach a threshold where they become sufficiently brittle to fracture under the repeated impacts of the milling balls. At this stage, fracture emerges as the primary mechanism for both components in the mixture. This shift results in a continuous reduction in D50 particle size beyond the 12-hour mark. Eventually, around

22 hours later, a steady state is approached, where the opposing effects of welding and fracturing reach a dynamic equilibrium, and further significant changes in particle size become minimal.

The incorporation of stearic acid as a Process Control Agent plays a significant role in maintaining this behavior. The effect of PCA on the size reduction process using the mechanical milling method has been well documented by several previous researchers [44,45]. Functioning as a surface-active compound, stearic acid adheres to the surface of powder particles, forming a thin layer. This layer effectively limits excessive cold welding, thereby encouraging the desired fracture of the particles during processing. In this study, cold welding initially plays the primary role, but the PCA effectively hinders excessive agglomeration. After 12 hours of milling, the dominant mechanism shifts, indicating a change in the process dynamics.

For powders primarily composed of ductile materials, milling without PCA can lead to substantial cold welding, making the size reduction process ineffective. Conversely, increasing the amount of PCA used enhances the dominance of the fracture mechanism in the particle size reduction process, thereby improving its effectiveness. However, the primary concern with using PCA, particularly stearic acid, in large quantities is that it significantly contributes to impurities in the coating. Thus, the appropriate use of PCA in this work was believed to positively influence the size reduction mechanisms in the milling process of both composite powder compositions.

As milling continues, the composite particles become progressively more uniform and refined. This improvement is evident in the EDS elemental distribution maps shown in Figure 4, where the elements appear increasingly well-dispersed.

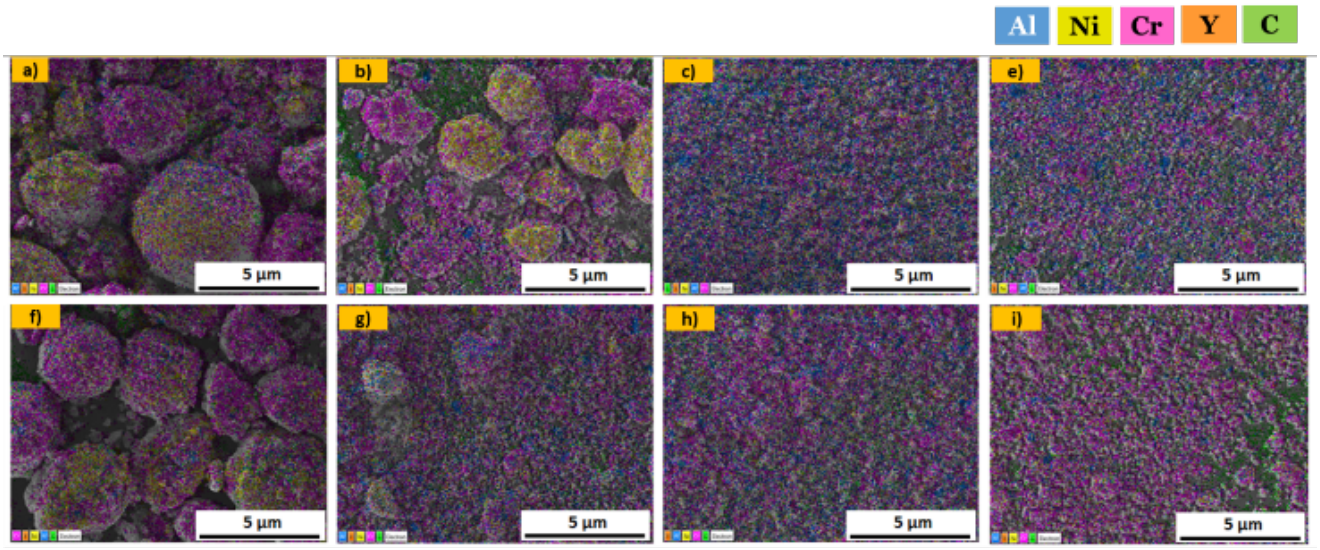

Fig. 4: Elements distribution mapping obtained from EDS analysis of the composite feedstock powder for (a) A(2), (b) A(12), (c) A(22), (d) A(36), (e) B(2), (f) B(12), (g) B(22), and (h) B(36).

After 2 hours, the elemental distribution remains quite uneven, and the original powders are still easily distinguishable. By the 36th hour, though, a significant transformation is evident: nickel, chromium, aluminum, and carbon are distributed much more uniformly throughout the particles. Achieving this level of homogenization is crucial for ensuring that the resulting coating has a uniform and reliable microstructure.

3.2 Phase analysis of the Milled Composite Feedstock Powder

Mechanical milling induces severe plastic deformation that not only alters the powder morphology but also generates significant transformations at the atomic and crystalline structure. Figure 5 shows the X-ray diffraction curve of the milled powder over a duration of 2 to 36 hours, providing insight into the transformations of the powder structure and phases.

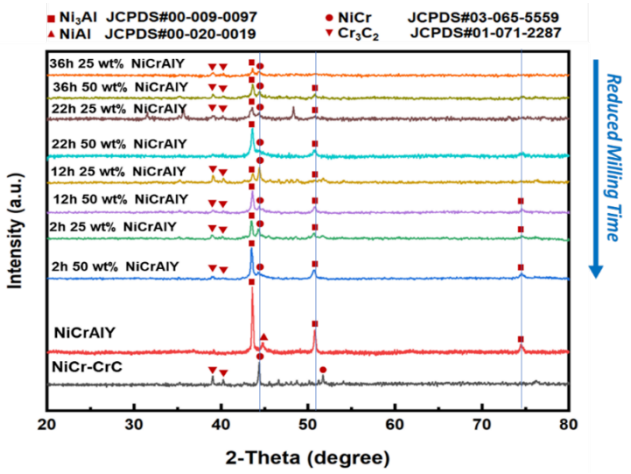

Fig. 5: X-ray diffraction curve of the milled composite powder

The as-received NiCrAlY powder X-ray diffraction curve displays the main peaks corresponding to the Ni3Al (γ') and NiAl (β) phases. The primary phase Ni3Al (γ') features a cubic FCC crystal structure, whereas the NiAl (β) phase is an intermetallic compound with a CsCl (cubic) structure.[46-48] The as-received NiCr-CrC powder shows prominent peaks at 2θ values of approximately 44.5 and 52 degrees, representing the NiCr phase. Other peaks correspond to the Cr_3C_2 phase. In the NiCr-CrC powder alloy, the NiCr phase serves as a matrix with an FCC crystal structure, while the Cr_3C_2 carbide reinforcement exhibits an orthorhombic crystal structure, with carbon atoms positioned at the center of the trigonal prism and chromium atoms occupying the corners of the prism.[49,50]

Notable observation in the XRD curve of all milled composite powders, regardless of their specific composition or duration of milling, is the absence of the NiAl (β) phase. This absence can be attributed to the dissolution of the NiAl (β) into the matrix Ni_3Al (γ') phase, facilitated by the severe plastic deformation process.[28,51] The mechanically induced phase transformation through a high amount of energy and defects facilitates the dissolution of the thermodynamically less stable NiAl (β) phase into the more stable Ni_3Al (γ') phase structure.

During the milling process, the crystalline grains undergo significant refinement, which is clearly reflected by the noticeable broadening of the XRD peaks as the milling time increases. The changes in peak width provide direct evidence of the grain refinement. This phenomenon can be assessed through the calculation of the crystallite size and lattice strain utilizing the Debye-Scherrer method.[52] The results of the crystal size calculations and lattice strain measurements using this method are illustrated in Figure 6 below.

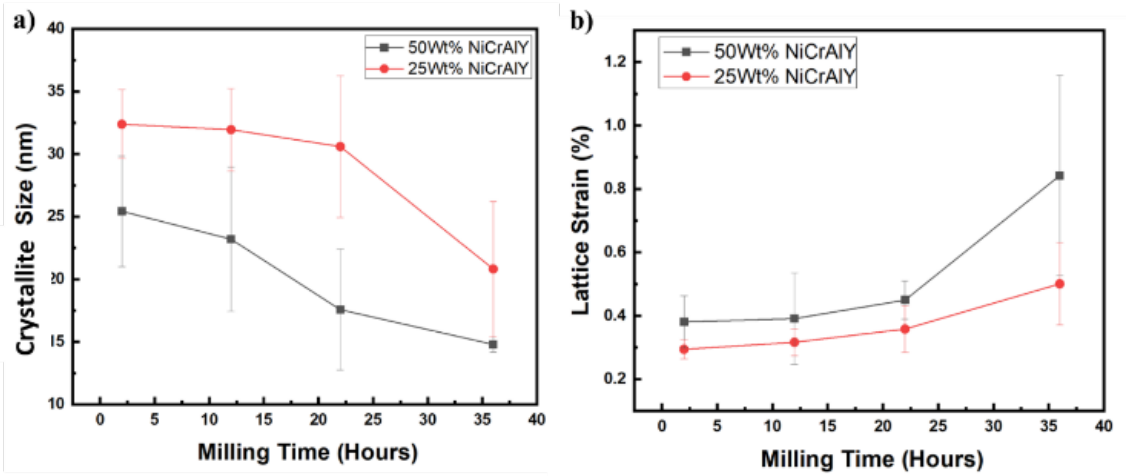

Fig. 6: a) Crystallite size of the composite feedstock powders; b) Lattice strain of the composite feedstock powder

The determination of the crystallite size and the measurements of the lattice strain with the Debye Scherrer method use the following equation:

$$D_{hkl} = \frac{K\lambda}{\beta_{hkl} \cos\theta}$$

D_hkl is the crystallite size, K is a numerical factor that correlates with particle shape. For nearly spherical particles, the K value is 0.98. λ is the wavelength of Cu-kα radiation from the incident X-rays (λ = 0.15406 nm). β_{hkl} refers to the width of the X-ray diffraction peak in radians (FWHM), while θ is the Bragg angle.

The results of the Ni_3Al crystallite size are presented in Figure 6. With extended milling time for both compositions A(n) and B(n), crystallite size progressively decreases, reaching values below 20 nm after 36 hours. Concurrently, the lattice strain ramps up, reflecting the accumulation of crystal defects, such as dislocations, that arise from deformation. The milling process can cause powder deformation, generating dislocations that are arranged into low-angle grain boundaries (LAGBs).[53,28] As deformation continues, these LAGBs gradually transform into high-angle grain boundaries. This process effectively fragments the original coarse grains, leading to the formation of a fine, randomly oriented nanocrystalline structure.

The rate of crystallite size reduction of the A(n) powder, which contains 50% NiCr-CrC, occurs at a notably greater rate compared to the B(n) powder with 75% NiCr-CrC. This difference is primarily attributed to the active deformation mechanisms present in each composition. The A(n) sample, with its higher content of ductile NiCrAlY phase, facilitates more pronounced deformation and dislocation multiplication within the metallic matrix, thereby promoting more effective grain refinement. In contrast, the B(n) sample, characterized by a greater proportion of the hard, brittle carbide phase, tends to absorb more of the milling energy through the fracture of these particles. As a result, the reduction in crystallite size is less efficient in B(n) compared to A(n).

3.3 Characterization of Coating

The properties of the feedstock powder have a crucial role in determining the microstructure and overall quality of the resulting coating. Figure 7 illustrates the microstructure of each coating corresponding to the respective milling process parameters.

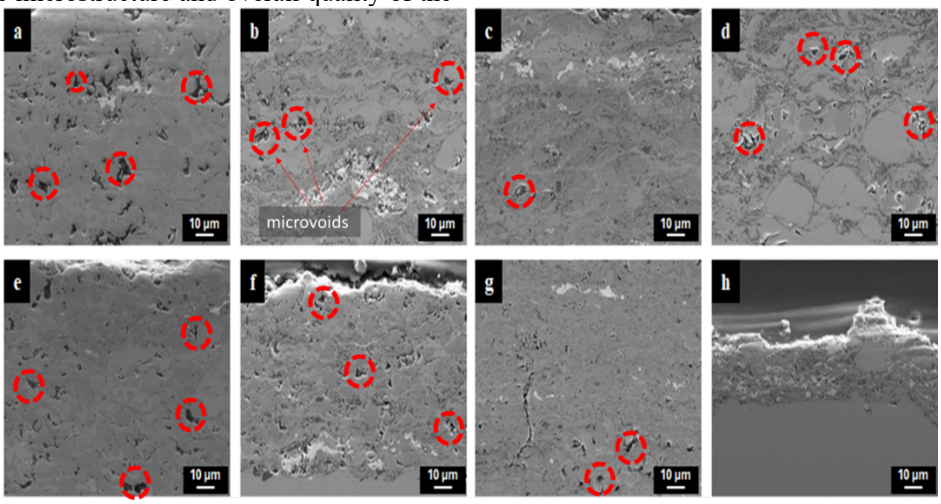

Fig. 7: Cross-sectional microstructure observation of the composite feedstock powder (a) A(2), (b) A(12), (c) A(22), (d) A(36), (e) B(2), (f) B(12), (g) B(22), and (h) B(36).

In Figure 7, the cross-sectional SEM images clearly display the typical characteristic of lamellar architecture of thermally sprayed coatings, with multiple overlapping, solidified splats forming the layered structure. The microstructure of the coatings formed from powders that are milled for extended periods tends to be less densely packed, exhibiting a higher degree of defects, such as pores and distinct inter-splat boundaries. Figure 8 presents the results of the microstructural analysis of powder B(12) using SEM. In this figure, elemental mapping was conducted to determine the distribution of elements in the coating. Additionally, EDS point analysis was performed to ascertain the composition of the phases detected with BSE in the SEM images.

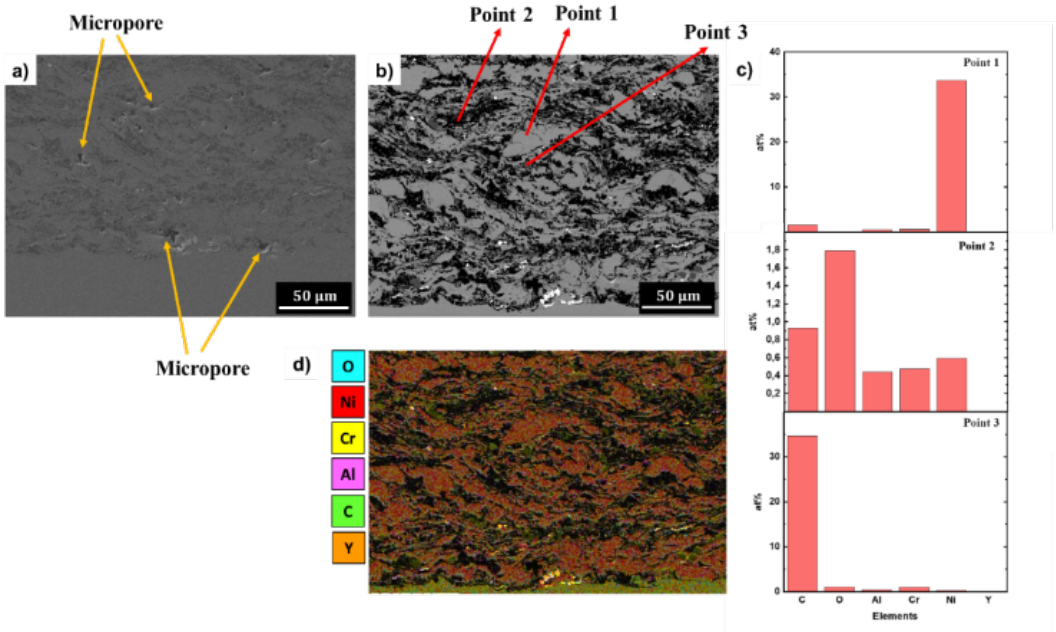

Fig. 8: SEM and EDS analysis of the coating cross-section

The SEM observation in Figure 8 indicates that only a few micropores are present in the coating microstructure. Furthermore, based on the EDS elemental analysis and BSE image of the cross-sectional coating microstructure, it is evident that the coating comprises at least three main regions: the light grey region (point 1), which dominantly consists of Ni; the dark grey region (point 3), which is near the carbide composition; and the black region (point 2), often appearing as thin, dark stringers along the splat boundaries, which is close to the oxide composition. This

observation is closely associated with in-flight particle oxidation, as in-flight oxidation tends to occur with decreasing particle size [54]. During the deposition process, the formation of volatile Cr_2O_3 may occur, and this oxide could also be present in the coating microstructure. Chemical interactions between the surface of the powder and oxygen create a layer of oxide on the molten powder during flight. These oxides begin to harden at the end of the flight, forming a thin oxide shell surrounding the droplet.

The oxygen concentration in the deposited coatings, as confirmed by EDS analysis and presented in Figure 9, shows a clear and significant increase with increasing milling time. This observation provides strong evidence that in-flight oxidation is actively occurring during the process. Essentially, the data establish a direct connection between extended powder milling and heightened oxidation, a crucial mechanism that influences the structural behavior of coatings. The mechanisms are significantly influenced by the particle size reduction achieved through milling. Figure 4 clearly demonstrates that prolonged milling results in a notable decrease in average particle size. As these particles become smaller, their surface-area-to-volume ratio increases significantly compared to larger counterparts. When these particles are introduced into the HVOF, they are subjected to intensely high temperatures and an oxygen-rich combustion environment. Smaller particles, due to their greater surface area relative to mass, absorb heat much more quickly than larger ones. As a result, these smaller particles can rapidly reach higher peak temperatures compared to the larger particles under the same conditions. With an increased reactive surface area and elevated particle temperatures, oxidation becomes significantly more pronounced as particles travel from the gun to the substrate. This results in the formation of an oxide shell, primarily consisting of Al_2O_3 and Cr_2O_3 as the most thermodynamically stable oxides within this system, on the surface of the molten or semi-molten droplets. Notably, prolonged milling time directly correlates with increased oxide composition, which accounts for the trend illustrated in Figure 9.

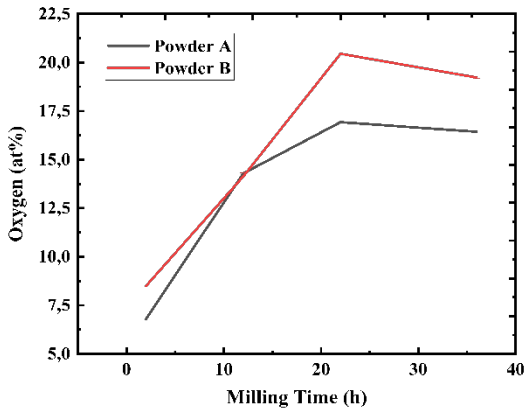

Fig. 9: Oxygen concentration in the composite coating as a function of milling time

The In-flight oxidation significantly deteriorates the coating structure in two major ways. First, the oxide shell that develops on the surface of the impacting droplets restricts their ability to plastically deform and flow. As a result, the molten material is unable to properly fill the surface irregularities, leading to porosity and weakly bonded splat boundaries. This result is clearly visible in the microstructures of over-milled powders. Second, the oxide layer acts as a physical barrier, preventing the direct, clean metallurgical contact required for strong inter-splat bonding. In addition, when particles are highly oxidized, they tend to be relatively brittle, which may cause them to fail to adhere upon impact, leading to reduced deposition efficiency. Thus, the In-flight oxidation may impair the effectiveness of the deposition process. Oxidation can occur during thermal spray coating, both in-flight and post-impact [55]. However, in-flight oxidation is the predominant mechanism for the inclusion of oxide in fine powder particles, resulting in a high oxygen concentration.

3.4 Hardness Evaluation

The microhardness of the coating is shown in Figure 10, accompanied by Tukey paired comparison analysis. The milling process appears to significantly influence the coating hardness, as indicated by the Tukey test ($P < 0.05$). Interestingly, this study demonstrates that as the powder particle size reduced, the hardness of the resulting coating decreased. Although previous studies have suggested that nanostructured carbide base powder produces coatings with superior hardness, owing to the Hall-Petch effect [56]. This finding suggests that a complex interplay of factors occurs during the HVOF process.

Smaller particles possess a higher surface-area-to-volume ratio, which enables them to absorb heat much faster. At the same time, however, the particles became far more vulnerable to oxidation as they passed through the high-temperature, oxygen-rich spray environment. Previous studies have shown this effect to be quite significant [57]; for instance, under identical spray conditions, a fine powder fraction (5 – 25 µm) produces a coating with over ten times the oxide content (22.8%) relative to the coarser fraction (25 – 38 µm), which contained only 1.8% oxides. The presence of these oxide networks significantly influences the coating's underlying cohesive strength. The oxide introduces inherent defects and serves as planes of weakness, which prevent the formation of appropriate metallurgical bonds between metallic splats.

During microhardness indentation testing, the applied stress tends to concentrate along these vulnerable interfaces. This concentration of stress promotes micro-fracturing and delamination, as opposed to facilitating plastic deformation within the metallic matrix. Consequently, the measured hardness is noticeably lower because the coating's structural integrity and cohesion are severely compromised. High oxide content leads to embrittlement between splats, resulting in a brittle and weak coating. This inter-splat

degradation completely impairs any potential Hall-Petch strengthening.

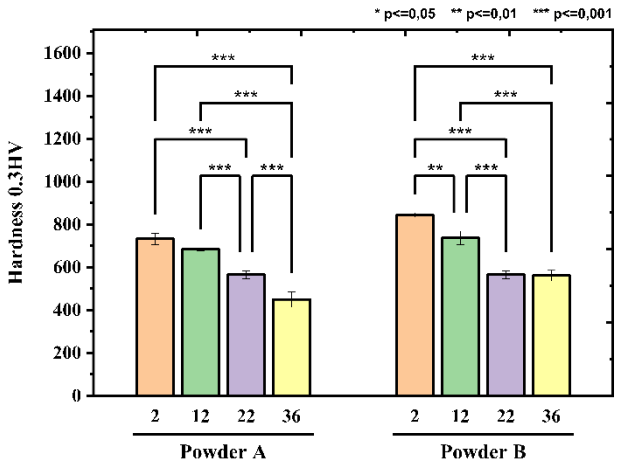

Fig. 10: Microvicker hardness with Tukey's paired comparison test of the composite coating

Further analysis of the effect of powder composition and milling time on coating hardness was conducted using ANOVA and the Fisher test. This methodology allows for assessing the examined factors, specifically powder composition and milling time. The results yielded by these tests are reported in Table 4.

Table 4: Two-way ANOVA analysis results of hardness test

	DF	Sum of Squares	Mean Square	F Value	P Value
Powder	1	26762,72435	26762,72435	45,98189	<0,0001
Milling Time	3	277791,5326	92597,17754	159,09415	<0,0001
Interaction	3	12361,06221	4120,35407	7,07931	0,00346
Model	7	303516,0569	43359,4367	74,49722	<0,0001
Error	15	8730,41325	582,02755		
Corrected Total	22	312246,4702			

The ANOVA analysis clearly highlights some findings. Both the powder composition ($F = 45.98$, $p < 0.0001$) and milling time ($F = 159.09$, $p < 0.0001$) exhibit significant main effects on microhardness, confirming that both variables independently exert considerable influence over the coating properties. Notably, the statistically significant interaction effect ($F = 7.08$, $p = 0.00346$) indicates that the impact of one factor depends upon the level of the other factor. In the physical context, this means that the reduction in hardness associated with longer milling times varies depending on the powder composition. This interaction effect quantitatively supports the observed behavioral differences, indicating that one powder composition is more susceptible to adverse effects such as increased in-flight oxidation and inter-splat embrittlement during prolonged milling than the other. The statistical analysis thus captures the interplay between powder composition and milling duration.

The statistical analysis provides clear insight into the complex relationship between material properties and processing conditions. Coatings produced from Powder B exhibit relatively higher hardness, primarily attributed to their elevated intrinsic carbide content, which serves as a principal strengthening phase. The ANOVA results indicate a significant interaction effect, suggesting that the rate of hardness reduction is intrinsically tied to the specific powder composition. This observation supports the underlying physical model, wherein each powder displays a distinct tendency to form an embrittling inter-splat oxide network, which is a factor that ultimately dictates the mechanical integrity of the coating.

3.5 Hardness Evaluation

The dry sliding behavior of the composite coating is illustrated in Figure 11, which compares the weight loss. The weight loss of the coated substrate generally increased with longer milling times during the powder preparation process. The Tukey test analysis indicates that the milling process significantly influenced the wear behavior of powder A's. The statistical significance value ($p < 0.05$) is evident in comparisons between 2 and 36 hours, as well as between 12 and 36 hours. In contrast, the weight loss difference for powder B as a function of milling time was not statistically significant ($p>0.05$).

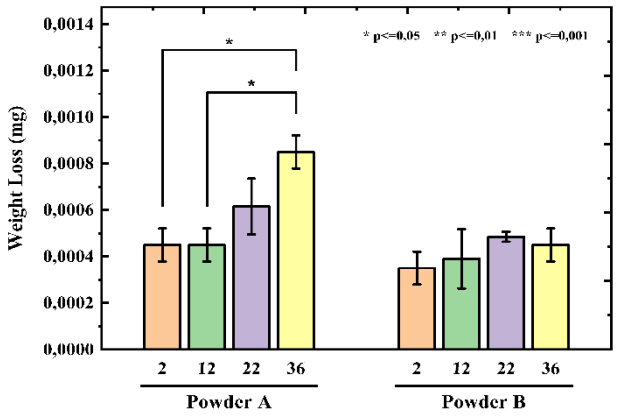

Fig. 11: Tukey's paired comparison test of the composite coating weight loss after the wear test

The results were evaluated using a two-way ANOVA and the Fisher test to analyze the influence of each factor on the coating's wear behavior. The findings from this analysis are presented in Table 5. The results indicate that wear behavior is strongly influenced by both powder composition and milling time ($p < 0.05$). However, no significant interactions were found between the powder composition and milling time ($p > 0.05$).

Table 5: Two-way ANOVA analysis results of wear behavior

	DF	Sum of Squares	Mean Square	F Value	P Value
Powder	1	1,19E-07	1,19E-07	16,97326	0,00334
Milling Time	3	1,65E-07	5,51E-08	7,85264	0,00907
Interaction	3	7,15E-08	2,38E-08	3,3975	0,07398
Model	7	3,56E-07	5,08E-08	7,24624	0,00606
Error	8	5,61E-08	7,01E-09		
Corrected Total	15	4,12E-07			

Mechanical milling eventually reduces the carbide particle size and disperses the particles uniformly. Nevertheless, decreasing the carbide grain size could also reduce the binder mean free path, which hinders slipping and suppresses dislocation propagation [58]. This structure exhibits behavior similar to work hardening in metals. As long as the accumulated stresses remain below the yield strength and do not induce fractures, reducing the binder's mean free path may positively enhance wear performance. However, further reduction may increase stress development during deformation or loading. Under these conditions, binder deformation becomes limited, generating high stresses that, with additional loading, cause individual carbide particles to interact, resulting in internal carbide stresses. This elevated stress level can lead to premature yielding or fracturing of the material or the individual carbides, which can adversely affect wear performance. Moreover, excessive grain refinement also results in a high-volume fraction of grain boundaries, can act as rapid diffusion channels for oxidizing species, potentially compromising the coating's environmental stability [59].

The inferior abrasive wear behavior in the over-milled powder is caused by the combination of factors working against material integrity. When the powder is milled past a certain threshold, excessively high internal stresses build up. Furthermore, overlaying this mechanical fragility is a prevalent oxide network, which is distributed through the microstructure. This oxide introduces embrittlement between splats, resulting in a brittle and inferior coating.

The interplay between composition and milling duration shapes the final properties of the composite powder and its coatings. The composition determines the relative hardness and brittleness of the phases involved, influencing how they respond to the milling process. The milling duration affects how these phases are fractured or deformed, influencing particle size, crystallite size, and the formation of oxide phases during the HVOF deposition process. Together, these factors determine the mechanical properties of the coatings, including hardness and wear resistance.

In other words, composition sets the foundational behavior of the powder during milling, whereas milling duration influences how that behavior translates into variations in microstructure and mechanical properties. The correct balance of these two factors is crucial for optimizing powder characteristics and achieving the desired performance in coatings.

4 Conclusions

This study investigates how variations in the composition of XNiCrAlY + Y(NiCr-CrC) composite coatings powder and milling time influence the microstructure, hardness, and wear resistance of coatings produced by the High-Velocity Oxygen-Fuel (HVOF) process. The results highlight the crucial role of both composition and milling time in determining the performance of the coatings, providing essential insights for optimizing these factors in industrial applications.

Powder composition plays a crucial role in the overall performance. Coatings with a higher carbide content (75 wt.% NiCr-CrC) exhibited a superior baseline of microhardness and wear resistance compared to those with 50 wt.% NiCr-CrC. The optimal processing window is identified as 2 to 8 hours, produced coatings with optimal microstructure and performance as the milling process refined the particle size. Beyond 12 hours, Powder A (50 wt.% (NiCr-CrC)) oxygen reach 17 at% with a 7% hardness loss (~730 HV to ~680 HV). For Powder B (75 wt% NiCr-CrC), this limit is more critical as oxygen surpasses 20 at%, causing a sharper 13% hardness loss (~840 HV to ~730 HV). Excessive milling triggers a statistically significant decline in properties, marking the onset of deleterious in-flight oxidation, negatively impacting the coatings' hardness, wear resistance, and powder deposition effectiveness.

These findings underscore that the interplay between powder composition and milling duration significantly influenced the wear behavior of the composite coatings. Smaller carbide grains enhanced wear resistance up to a threshold beyond which further refinement led to a decline in performance. These findings demonstrate the importance of controlling milling conditions to preserve carbide integrity and optimize coating properties.

Conflicts of Interest Statement

The authors certify that they have NO affiliations with or involvement in any organization or entity with any financial interest (such as honoraria; educational grants; participation in speakers' bureaus; membership, employment, consultancies, stock ownership, or other equity interest; and expert testimony or patent-licensing arrangements), or non-financial interest (such as personal or professional relationships, affiliations, knowledge or beliefs) in the subject matter or materials discussed in this manuscript.

References

[1] B. Zheng, S. Wang, and J. Xu, A Review on the CO2 Emission Reduction Scheme and Countermeasures in China’s Energy and Power Industry under the Background of Carbon Peak, Sustainability, **14**(2022) 879.

[2] A.Di Gianfrancesco. 1 - The fossil fuel power plants technology, in Materials for Ultra-Supercritical and Advanced Ultra-Supercritical Power Plants, Woodhead Publishing, 1-49, (2017)

[3] A.Husain, and K. Habib, Investigation of tubing failure of super-heater boiler from Kuwait Desalination Electrical Power Plant, Desalination, **183**(2005) 203-208.

[4] G. Prashar, and H. Vasudev, Structure-property correlation and high-temperature erosion performance of Inconel625-Al2O3 plasma-sprayed bimodal composite coatings, Surface and Coatings Technology, **439**(2022) 128450.

[5] A.Kumar, and P. K. Sapra, Tribological characterisation of SA210 Gr A1 boiler steels for different temperature applications, International Journal of Surface Science and Engineering, **10**(2016) 375-388.

[6] P. K. Sapra, S. Singh, and S. Prakash, Erosion-corrosion behaviour of Ni-based superalloy Superni-600 in the real service environment of the boiler, International Journal of Microstructure and Materials Properties, **5**(2010) 536-547.

[7] S. Yoneda, S. Hayashi, Y. Miyakoshi, T. Kogin, E. Ishikawa, and M. Noguchi, Erosion-corrosion behavior of Ni-20Cr-4Fe and Ni-20Cr-4Fe-7Mo under fluidized-bed biomass boiler conditions, Corrosion Science, **205**(2022) 110472.

[8] K. Szymański, A. Hernas, G. Moskal, and H. Myalska, Thermally sprayed coatings resistant to erosion and corrosion for power plant boilers - A review, Surface and Coatings Technology, **268**(2015) 153-164.

[9] P. L. Fauchais, J. V. R. Heberlein, and M. I. Boulos. Nanostructured or Finely Structured Coatings, in Thermal Spray Fundamentals: From Powder to Part, Springer US, Boston, MA: 981-1111, (2014)

[10] V. Higuera Hidalgo, J. Belzunce Varela, A. Carriles Menéndez, and S. Poveda Martínez, High temperature erosion wear of flame and plasma-sprayed nickel–chromium coatings under simulated coal-fired boiler atmospheres, Wear, **247**(2001) 214-222.

[11] M. Kašparová, F. Zahálka, and Š. Houdková, WC-Co and Cr3C2-NiCr Coatings in Low- and High-Stress Abrasive Conditions, Journal of Thermal Spray Technology, **20**(2011) 412-424.

[12] Š. Houdková, F. Zahálka, M. Kašparová, and L. M. Berger, Comparative Study of Thermally Sprayed Coatings Under Different Types of Wear Conditions for Hard Chromium Replacement, Tribology Letters, **43**(2011) 139-154.

[13] L. Janka, J. Norpoth, S. Eicher, M. Rodríguez Ripoll, and P. Vuoristo, Improving the toughness of thermally sprayed Cr3C2-NiCr hardmetal coatings by laser post-treatment, Materials & Design, **98**(2016) 135-142.

[14] L. Vilhena, B. Domingues, C. Fernandes, A. Senos, and A. Ramalho, Mechanical and Tribological Characterization of WC-Co and WC-AISI 304 Composites by a Newly Developed Equipment, Materials, **15**(2022) 1187.

[15] B. Casas, X. Ramis, M. Anglada, J. M. Salla, and L. Llanes, Oxidation-induced strength degradation of WC–Co hardmetals, International Journal of Refractory Metals and Hard Materials, **19**(2001) 303-309.

[16] H. Warlimont. Ceramics, in Springer Handbook of Condensed Matter and Materials Data, Springer Berlin Heidelberg, Berlin, Heidelberg: 431-476, (2005)

[17] F. Goodwin, S. Guruswamy, K. U. Kainer, C. Kammer, W. Knabl, A. Koethe, G. Leichtfried, G. Schlamp, R. Stickler, and H. Warlimont. Metals, in Springer Handbook of Condensed Matter and Materials Data, Springer Berlin Heidelberg, Berlin, Heidelberg: 161-430, (2005)

[18] W.-c. Zhang, L.-b. Liu, M.-t. Zhang, G.-x. Huang, J.-s. Liang, X. Li, and L.-g. Zhang, Comparison between WC–10Co–4Cr and Cr3C2–25NiCr coatings sprayed on H13 steel by HVOF, Transactions of Nonferrous Metals Society of China, **25**(2015) 3700-3707.

[19] M. Ksiazek, L. Boron, M. Radecka, M. Richert, and A. Tchorz, Mechanical and Tribological Properties of HVOF-Sprayed (Cr3C2-NiCr+Ni) Composite Coating on Ductile Cast Iron, Journal of Materials Engineering and Performance, **25**(2016) 3185-3193.

[20] G. Padmavathi, B. N. Sarada, S. P. Shanmuganathan, B. V. Padmini, and N. Mohan, Effects of high velocity oxy fuel thermal spray coating on mechanical and tribological properties of materials–A review, Materials Today: Proceedings, **27**(2020) 2152-2157.

[21] N. Espallargas, J. Berget, J. M. Guilemany, A. V. Benedetti, and P. H. Suegama, Cr3C2–NiCr and WC–Ni thermal spray coatings as alternatives to hard chromium for erosion–corrosion resistance, Surface and Coatings Technology, **202**(2008) 1405-1417.

[22] S. Hong, Y. Wu, Q. Wang, G. Ying, G. Li, W. Gao, B. Wang, and W. Guo, Microstructure and cavitation–silt erosion behavior of high-velocity oxygen–fuel (HVOF) sprayed Cr3C2–NiCr coating, Surface and Coatings Technology, **225**(2013) 85-91.

[23] S. Septianissa, B. Prawara, E. A. Basuki, E. Martides, and E. Riyanto, Improving the hot corrosion resistance of γ/γ' in Fe-Ni superalloy coated with Cr3C2-20NiCr and NiCrAlY using HVOF thermal spray coating, International Journal of Electrochemical Science, **17**(2022) 221231.

[24] S. Septianissa, and A. Z. Chandrasari, Behavior of Bare, Cr3C2-20NiCr, and NiCrAlY coated Fe-Ni Based Superalloy Under Hot Corrosion in a 75 wt.% Na2SO4 + 25wt.% NaCl film at 900^{0}C, International Journal of Science and Society, **6**(2024) 11.

[25] B. Li, S. Ma, Y. Gao, C. Li, H. Guo, Q. Zheng, Y. Kang, and J. Jia, Mechanical, Tribological, and

Oxidation Resistance Properties of NiCrAlY Coating by Atmospheric Plasma Spraying, Frontiers in Materials, **6**(2019).

[26] N. Jegadeeswaran, M. R. Ramesh, and K. U. Bhat, Combating Corrosion Degradation of Turbine Materials Using HVOF Sprayed 25% (Cr3C2-25(Ni20Cr)) + NiCrAlY Coating, International Journal of Corrosion, (2013).

[27] K. Anand Babu, N. Jegadeeswaran, H. S. Nithin, and N. Kapilan, Studies on solid particle erosion by HVOF sprayed 25% (Cr3C2-25 (Ni20Cr)) + 75% NiCrAlY on Ti-31, Materials Today: Proceedings, **45**(2021) 246-253.

[28] M. Tahari, M. Shamanian, and M. Salehi, Microstructural and morphological evaluation of MCrAlY/YSZ composite produced by mechanical alloying method, Journal of Alloys and Compounds, **525**(2012) 44-52.

[29] K. Tao, X. Zhou, H. Cui, and J. Zhang, Microhardness variation in heat-treated conventional and nanostructured NiCrC coatings prepared by HVAF spraying, Surface and Coatings Technology, **203**(2009) 1406-1414.

[30] G.-C. Ji, C.-J. Li, Y.-Y. Wang, and W.-Y. Li, Microstructural characterization and abrasive wear performance of HVOF sprayed Cr3C2–NiCr coating, Surface and Coatings Technology, **200**(2006) 6749-6757.

[31] K. Tao, J. Zhang, H. Cui, X.-l. Zhou, and J.-s. Zhang, Fabrication of conventional and nanostructured NiCrC coatings via HVAF technique, Transactions of Nonferrous Metals Society of China, **18**(2008) 262-269.

[32] C. Suryanarayana, A. A. Al-Joubori, and Z. Wang, Nanostructured Materials and Nanocomposites by Mechanical Alloying: An Overview, Metals and Materials International, **28**(2022) 41-53.

[33] M. Roy, A. Pauschitz, J. Wernisch, and F. Franek, The influence of temperature on the wear of Cr3C2–25(Ni20Cr) coating—comparison between nanocrystalline grains and conventional grains, Wear, **257**(2004) 799-811.

[34] J. He, and E. J. Lavernia, Precipitation phenomenon in nanostructured Cr3C2–NiCr coatings, Materials Science and Engineering: A, **301**(2001) 69-79.

[35] M. Daroonparvar, M. S. Hussain, and M. A. M. Yajid, The role of formation of continues thermally grown oxide layer on the nanostructured NiCrAlY bond coat during thermal exposure in air, Applied Surface Science, 261(2012) 287-297.

[36] W. Hu, M. Li, and M. Fukumoto, Preparation and properties of HVOF NiAl nanostructured coatings, Materials Science and Engineering: A, **478**(2008) 1-8.

[37] A.Tiwari, S. Seman, G. Singh, and R. Jayaganthan, Nanocrystalline Cermet Coatings for Erosion–Corrosion Protection, Coatings, **9**(2019) 400.

[38] K. J. Stein, B. S. Schorr, and A. R. Marder, Erosion of thermal spray MCr–Cr3C2 cermet coatings, Wear, **224**(1999) 153-159.

[39] B. He, L. Zhang, X. Yun, J. Wang, G. Zhou, Z. Chen, and X. Yuan, Comparative Study of HVOF Cr3C2–NiCr Coating with Different Bonding Layer on the Interactive Behavior of Fatigue and Corrosion, Coatings, **12**(2022) 307.

[40] B. Seitov, S. Kurbanbekov, D. Baltabayeva, D. Kakimzhanov, K. Katpayeva, A. Temirbekov, S. Bekbayev, and N. Mussakhan, Review of Physical and Mechanical Properties, Morphology, and Phase Structure in Cr3C2-NiCr Composite Coatings Sprayed by HVOF Method, Coatings, **15**(2025) 479.

[41] A.Alizadeh, E. Taheri-Nassaj, and H. R. Baharvandi, Preparation and investigation of Al–4 wt % B4C nanocomposite powders using mechanical milling, Bulletin of Materials Science, **34**(2011) 1039-1048.

[42] R. U. Din, Q. A. Shafqat, Z. Asghar, G. H. Zahid, A. Basit, A. H. Qureshi, T. Manzoor, M. A. Nasir, F. Mehmood, and K. I. Hussain, Microstructural Evolution, Powder Characteristics, Compaction Behavior and Sinterability of Al 6061–B4C Composites as a Function of Reinforcement Content and Milling Times, Russian Journal of Non-Ferrous Metals, **59**(2018) 207-222.

[43] W. Zhai, B. Pu, L. Sun, H. Dong, Y. Wang, H. Lin, and Y. Gao, Influence of Ni content on the microstructure and mechanical properties of chromium carbide-nickel composites, Ceramics International, **46**(2020) 8754-8760.

[44] Q. Han, R. Setchi, and S. L. Evans, Characterisation and milling time optimisation of nanocrystalline aluminium powder for selective laser melting, The International Journal of Advanced Manufacturing Technology, **88**(2017) 1429-1438.

[45] N. Yazdani, M. R. Toroghinejad, A. Shabani, and P. Cavaliere, Effects of Process Control Agent Amount, Milling Time, and Annealing Heat Treatment on the Microstructure of AlCrCuFeNi High-Entropy Alloy Synthesized through Mechanical Alloying, Metals, **11**(2021) 1493.

[46] J. A. Picas, A. Forn, L. Ajdelsztajn, and J. Schoenung, Nanocrystalline NiCrAlY powder synthesis by mechanical cryomilling, Powder Technology, **148**(2004) 20-23.

[47] V. Abhijith Vijay, K. Santhy, G. Sivakumar, and B. Rajasekaran, Thermal expansion and microstructure evolution of atmospheric plasma sprayed NiCrAlY bond coat using in-situ high temperature X-ray diffraction, Surface and Coatings Technology, **452**(2023).

[48] Y. Chen, X. Zhao, and P. Xiao, Effect of microstructure on early oxidation of MCrAlY coatings, Acta Materialia, **159**(2018) 150-162.

[49] A.H. Cottrell, Crystal structures of transition metal carbides, Materials Science and Technology, **11**(1995) 329-333.

[50] J. A. Picas, M. Punset, S. Menargues, M. Campillo, M. Teresa Baile, and A. Forn, The influence of heat treatment on tribological and mechanical properties of HVOF sprayed CrC–NiCr coatings, International Journal of Material Forming**, 2**(2009) 225.

[51] F. Ghadami, A. Sabour Rouh Aghdam, and S. Ghadami, A comprehensive study on the microstructure evolution and oxidation resistance of conventional and nanocrystalline MCrAlY coatings, Scientific Reports, **11**(2021) 875.

[52] H. P. Klug, and L. E. Alexander. (1974). X-Ray Diffraction Procedures: For Polycrystalline and Amorphous Materials, 2nd Edition.

[53] F. Karimzadeh, M. H. Enayati, and M. Tavoosi, Synthesis and characterization of Zn/Al2O3 nanocomposite by mechanical alloying, Materials Science and Engineering: A, **486**(2008) 45-48.

[54] N. Rana, R. Jayaganthan, and S. Prakash, Microstructural features and oxidation behavior of nano and conventional NiCrAlY coatings developed by LVOF process, Surface and Coatings Technology, **260**(2014) 28-33.

[55] C.-J. Li, and W.-Y. Li, Effect of sprayed powder particle size on the oxidation behavior of MCrAlY materials during high velocity oxygen-fuel deposition, Surface and Coatings Technology, **162**(2003) 31-41.

[56] L. Thakur, and N. Arora, Sliding and Abrasive Wear Behavior of WC-CoCr Coatings with Different Carbide Sizes, Journal of Materials Engineering and Performance, **22**(2013) 574-583.

[57] R. Saharkhiz, Z. Valefi, M. Mirjani, and A. Mirak, Comprehensive study on the effect of HVOF processing parameters and particle size on high-temperature properties of NiCoCrAlYTa coatings, Surface and Coatings Technology, **473**(2023) 129951.

[58] M. M. El Rayes, E.-S. M. Sherif, and H. S. Abdo, Comparative Study into Microstructural and Mechanical Characterization of HVOF-WC-Based Coatings, Crystals, **12**(2022) 969.

[59] Birbilis, N., Cavanaugh, M. K., & Buchheit, R. G. On the effect of microstructure and grain size on the corrosion and oxidation of metals. Corrosion Engineering, Science and Technology, **45**(2010), 224–230.